AIAA 93-2921

Interpretation of Waverider Performance Data Using Computational Fluid Dynamics

Charles E. Cockrell, Jr.
NASA-Langley Research Center
Hampton, VA

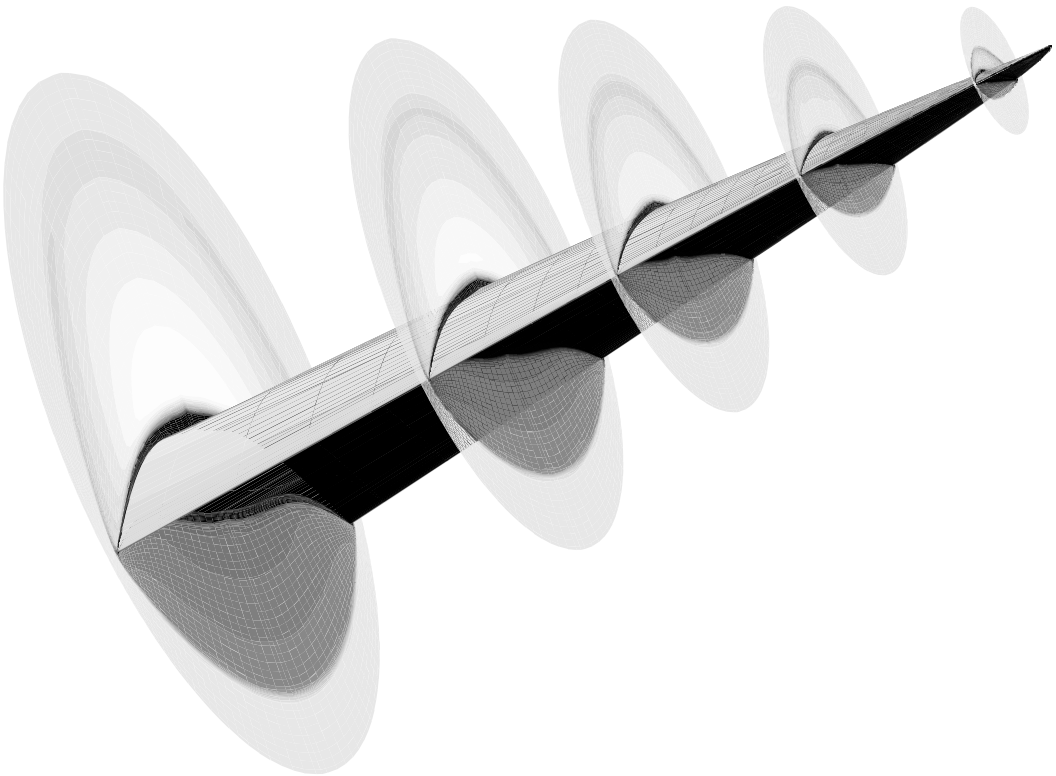

AIAA 24th
Fluid Dynamics Conference
July 6-9, 1993 / Orlando, FL

INTERPRETATION OF WAVERIDER PERFORMANCE DATA USING COMPUTATIONAL FLUID DYNAMICS

Charles E. Cockrell, Jr.*
NASA Langley Research Center
Hampton, VA

Abstract

A computational study was conducted to better understand experimental results obtained from wind tunnel tests of a Mach 4 waverider model and a comparative reference configuration. The experimental results showed that the performance of the reference configuration was slightly better than that of the waverider model. These results contradict waverider design theory, which suggests that a waverider optimized for maximum lift-to-drag should provide better performance than any other non-waverider configuration at a given design point, especially at hypersonic speeds. The computational results showed that the predicted surface pressure values and the integrated lift and drag coefficients from the pressure distributions were much lower for the reference model than for the flat-top model, due to the reference model bottom surface having a slight expansion. The lift-to-drag ratios for the flat-top model were higher due to a relatively low drag for the same amount of lift. These results indicate that the performance advantage of the reference model was due to the shape of the bottom surface and not due to the flat top surface. The results also showed that the reference model exhibited the same shock attachment characteristics as the waverider because the planform shapes were identical. CFD predictions show that the planform shape gives the waverider an advantage in performance over conventional hypersonic vehicles and that altering the bottom surface of a waverider does not cause significant performance degradation.

Nomenclature

α	angle of attack, degrees
C_L	lift coefficient
C_D	drag coefficient
X,Y,Z	coordinate axis system, inches
I,J,K	computational grid axes
M	Mach number
P	static pressure, lbf/ft^2
P_{base}	base pressure, lbf/ft^2
y^+	inner law variable

Subscripts

∞	freestream conditions

Introduction

Waveriders are candidate shapes for various types of hypersonic aircraft designs. A waverider is a shape designed from a known supersonic or hypersonic flow field, such as flow past a right circular cone.[1] The waverider is designed such that the bow shock is attached along the outer leading edge at the design point. A typical waverider design from a conical flow field is shown in figure 1. The lower surface is designed by using the known flow field to trace streamlines from the leading edge to the trailing edge. A waverider is uniquely defined by a leading edge definition and a specific set of freestream conditions. The upper surface may be designed as either a freestream surface or as a slight expansion surface to provide an additional contribution to lift. The shape is generally optimized for either maximum lift-to-drag ratio or minimum drag at the design point. The attached shock wave creates an efficient compression lifting surface with no flow spillage from the lower surface to the upper surface at the design point. Because of this characteristic, the predicted lift-to-drag ratios of waveriders are higher than those for conventional hypersonic vehicle concepts. The uni-

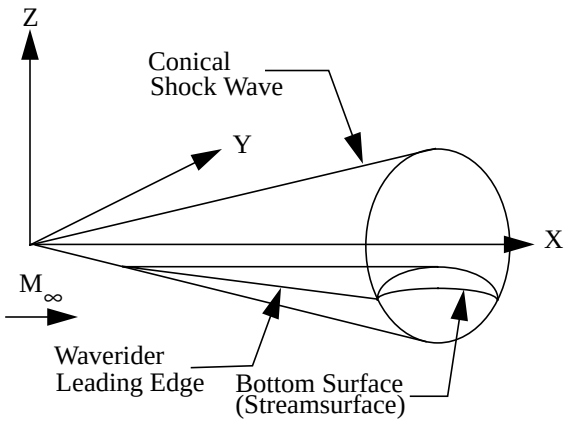

Figure 1. Waverider Designed From Conical Flow Field

* Aerospace Engineer, Supersonic/Hypersonics Aerodynamics Branch, Applied Aerodynamics Division, Member AIAA.

formity of the lower surface flow field and the absence of crossflow make the waverider an ideal candidate for scramjet propulsion system integration.[2]

Previous criticisms of waveriders have been resolved in recent studies,[1,3,4] leading to renewed interest in their use for hypersonic vehicle designs. One criticism is that early design techniques used only inviscid methods which produced shapes with large surface areas that resulted in large skin-friction drag. The lift-to-drag ratios obtained experimentally were poor compared to predictions. Current design codes include an estimate for skin-friction drag in the optimization process.[1] This improvement allows the optimization routine to minimize wetted surface area and provide more accurate estimates for aerodynamic performance. The class of vehicles designed using this method is called viscous-optimized waveriders. A second concern associated with waveriders is that their off-design performance may be poor even though on-design performance is excellent. However, recent experimental and computational studies have shown that waveriders which demonstrate acceptable off-design performance can be designed.[3,4] Additionally, optimization routines can include various volumetric constraints which allow for the design of shapes with improved volumetric efficiencies and packaging characteristics while accepting a minimum penalty in aerodynamic performance. Previous computational studies have validated design methods and predicted waverider flow-field properties accurately.[4]

An experimental program was conducted at NASA Langley Research Center to investigate the aerodynamic performance of a viscous-optimized waverider and a reference configuration.[3] A Mach 4 waverider and a flat-top reference configuration were tested in the Unitary Plan Wind Tunnel (UPWT). The design point of Mach 4 was chosen based on facility limitations and the desire to obtain data at, above and below the design Mach number. The reference configuration was intended to show the benefits of waverider flow-field properties by comparing a waverider to a non-waverider at the same conditions. The configurations were tested over an angle-of-attack range from -16^o to 14^o at Mach 4 and at off-design Mach numbers at zero angle of attack. This study showed that the maximum lift-to-drag ratio of the flat-top model was approximately 5 percent higher than that of the waverider model. This result was unexpected since theoretically the waverider should provide better performance than any other non-waverider configuration at the design point.

In order to better understand these experimental results, a computational study was conducted. The study consisted of obtaining computational fluid dynamics (CFD) solutions of both the waverider and the reference model flow fields. The results were used to interpret the wind tunnel data for the two models and to illustrate the benefits of waverider flow-field properties. This paper will present the details of the CFD study and limited comparisons with the experimental data.

Configuration Design

The waverider model was designed using the Maryland Axisymmetric Waverider Program (MAXWARP).[1,5] The MAXWARP code includes an estimate for skin friction in the optimization process, using the reference temperature method. The code also uses a simplex optimization algorithm to optimize shapes for maximum lift-to-drag ratio or minimum drag at the design point.[5] In this study, the waverider model was optimized for maximum lift-to-drag ratio at Mach 4.0. This is more appropriate as a hypersonic cruise performance parameter than minimum drag. The top surface was designed as an expansion surface using the axisymmetric method of characteristics. Some volumetric constraints were also incorporated into the optimization routine in order to increase volumetric efficiency and to generate a shape which had good structural characteristics for a wind tunnel model. These included a range for the base-height-to-length (fineness) ratio and a minimum volume. The cone semi-apex angle used to create the conical flow field was chosen to yield the highest maximum lift-to-drag ratio. An oblique view and a 3-view sketch of the waverider model is shown in figure 2.

The flat-top model was designed by adjusting the top surface coordinate of the waverider at each cross section to create a flat surface and then adjusting the corresponding bottom surface coordinate at that cross section by the same increment. The result is a non-waverider configuration with the same cross-sectional area distribution and planform shape as the waverider model. An oblique view and 3-view sketch of the reference model is shown in figure 3.

Computational Study

The computational study consisted of obtaining viscous solutions for both configurations using the General Aerodynamic Simulation Program (GASP), version 2.0.[6] GASP version 2.0 can solve the full Reynolds-averaged Navier-Stokes equations as well as subsets of these equations, including the thin-layer Navier-Stokes (TLNS), parabolized Navier-Stokes (PNS) and Euler equations. The solutions shown in this study were obtained by solving the TLNS equations in the nose region in order to capture the region of subsonic flow behind the bow shock and the PNS equations over the remaining configuration. Solutions were obtained for the waverider and flat-top configurations over an angle-of-attack range from 0^o to 10^o at Mach 4.0. Off-design solutions at Mach 3.5 and Mach 4.5 at 0^o angle of attack were obtained for the waverider only.

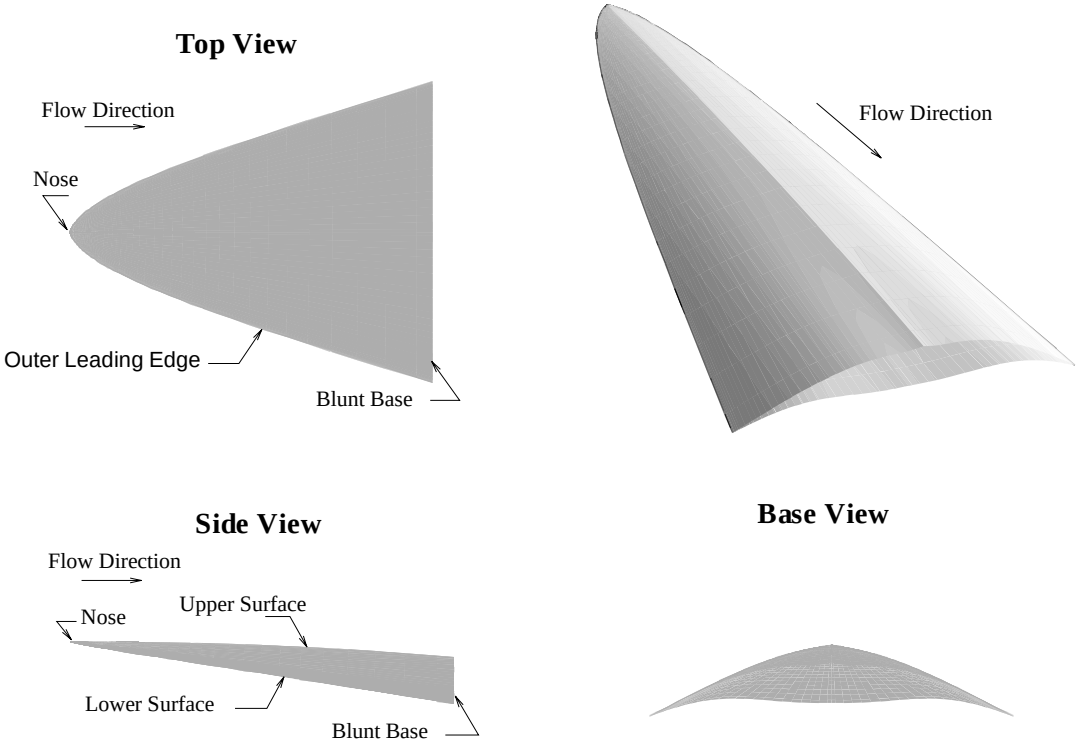

Figure 2. Mach 4 Waverider Model

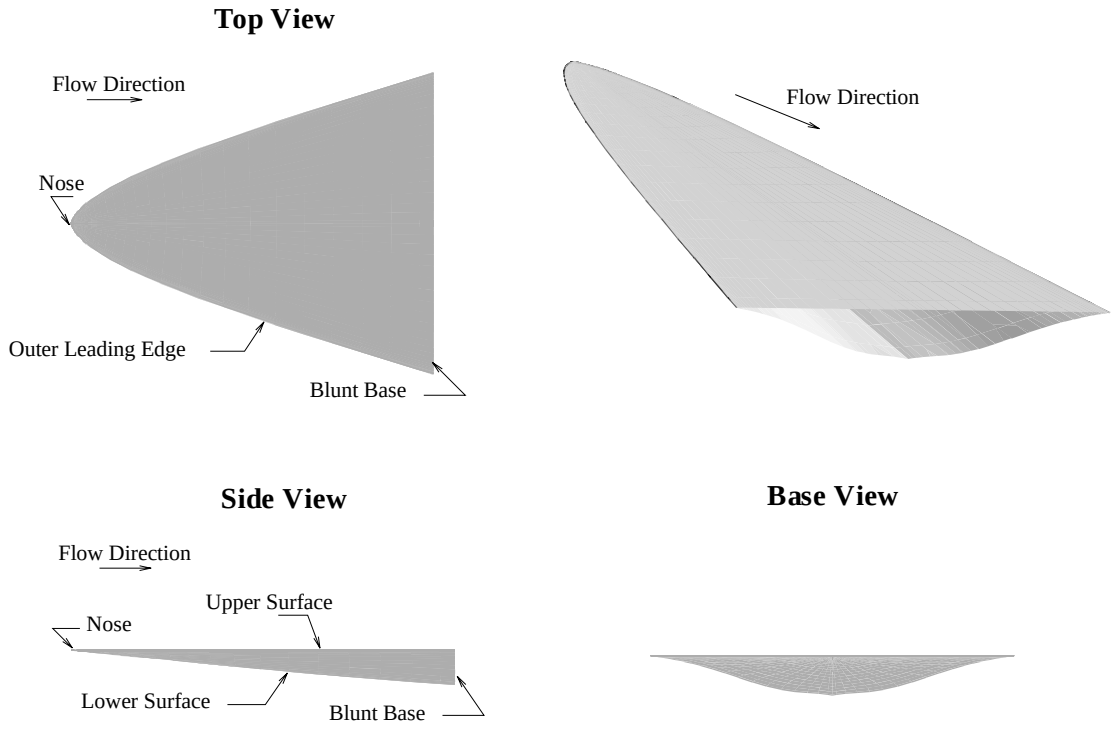

Figure 3. Mach 4 Reference Flat-Top Model

The numerical method in GASP is based on the upwind/relaxation algorithms. Time integration is based on the integration of primitive variables and uses a 2-factor approximate factorization scheme. Convergence to a steady state solution is accomplished by reducing the L2 norm of the residual by 4 orders of magnitude. Van Leer's flux-vector splitting algorithm is used with the exception that full flux is enforced in the marching direction for PNS solutions. Mesh sequencing is used to accelerate convergence for the TLNS solutions. A no-slip boundary condition with a fixed wall temperature of 324.67 K is imposed on solid boundaries.

The grid used for the waverider solutions was generated from a previous computational study which examined this configuration at the design Mach number only.[7] The grid was generated using an algebraic transfinite interpolation method and used an adaptive grid approach to cluster cells in the region of shock waves at the design point. The grid that was adapted for flow at Mach 4.0 and an angle of attack of 0^o is used for all of the solutions in this study. The waverider grid consisted of 53 points in the streamwise direction, 71 points in the circumferential direction, and 51 points in the vertical direction. The grid for the flat-top solutions was generated using algebraic transfinite interpolation methods with elliptic interior point refinement. These techniques were implemented by using the GRIDGEN software package.[8] The flat-top grid contained 51 points in the streamwise direction, 71 points in the circumferential direction, and 61 points in the vertical direction. Both grids had points clustered near the solid boundaries in order to adequately resolve boundary layers in viscous solutions. The amount of clustering required is determined by examining the inner law variable, y^+. Previous studies have shown that y^+ values on the order of 1.0 will yield an accurate solution.[9] A diagram of both the waverider and flat-top model grids is shown in figure 4.

Lift and drag coefficients were obtained by integrating pressures predicted by CFD solutions over the configuration surfaces and including an estimate for skin friction using the reference temperature method.[10] Additionally, two methods are used to account for the blunt base. The first method assumes a base pressure of zero while the second assumes a base pressure equal to freestream pressure. Lift and drag predictions are presented using both methods.

Results

The results from the computational study are presented in two parts. First, lift and drag coefficients from integrated surface pressure predictions are presented for the design Mach number of 4.0 and selected off-design Mach numbers. Second, flow-field solutions as well as lift and drag coefficients from integrated surface pressure predictions are presented for both the flat-top model and the waverider at

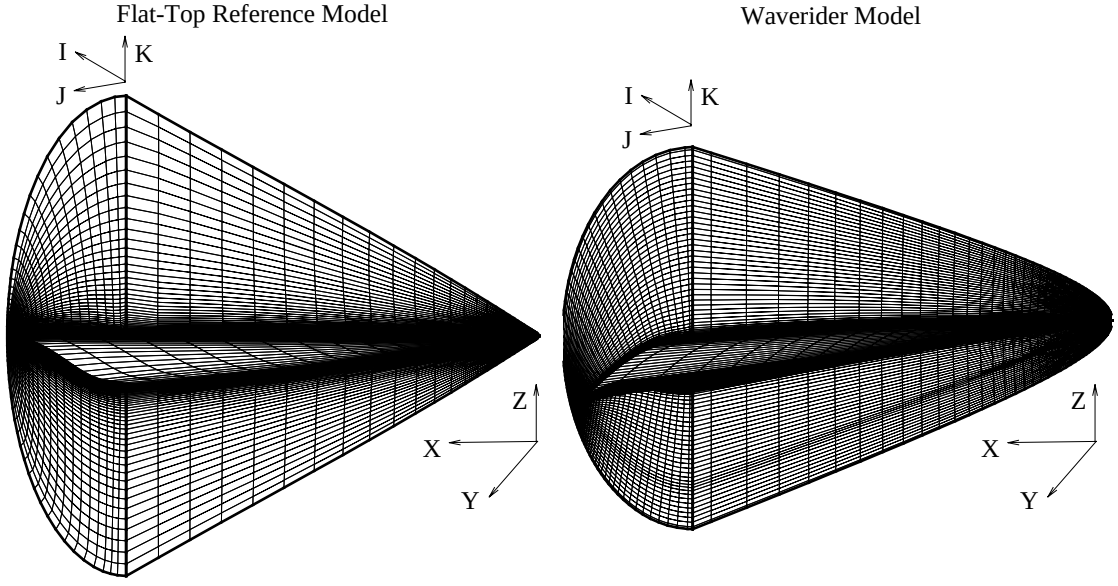

Figure 4. Grids for Waverider and Flat-Top Configurations

Mach 4.0 and various angles of attack. Comparisons of surface pressure predictions and performance characteristics of each configuration are made. Two different methods of accounting for the blunt base is also examined for both models. Comparisons between computational predictions and experimental data are presented for some cases. The experimental data were documented assuming that the base pressure is equal to freestream pressure. Therefore, comparisons are presented only for this case.

Lift and drag coefficients for the waverider model at 0^o angle of attack for the design Mach number of 4.0 and for off-design Mach numbers are shown in table 1. The predictions for lift coefficient, drag coefficient and lift-to-drag ratio are presented in figures 5, 6 and, 7. These results show that lift decreases as Mach number increases. Drag also decreases as Mach number increases for the case of base pressure equal to zero. However, for the case of base pressure equal to freestream pressure, the drag has a maximum value at Mach 4.0. Because of this difference, there is an opposite trend in the lift-to-drag ratios when comparing the two methods of base pressure correction. Assuming zero base pressure, the lift-to-drag ratio increases as Mach number increases. However, the lift-to-drag ratio decreases with increasing Mach number when freestream pressure at the base is assumed. In both cases, the lift-to-drag ratios presented agree with reference 3, which showed that the performance of waveriders does not degrade significantly at off-design conditions.

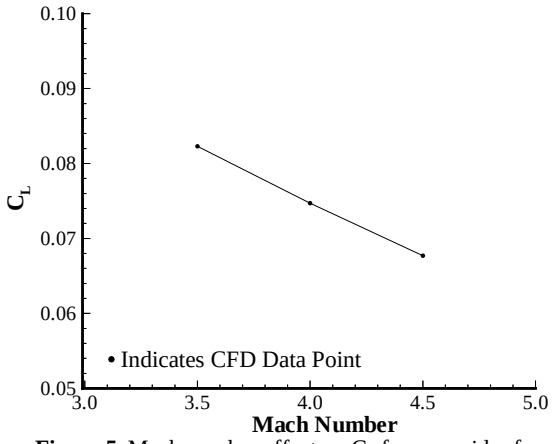

Figure 5. Mach number effect on C_L for waverider from CFD Predictions at α=0.0.

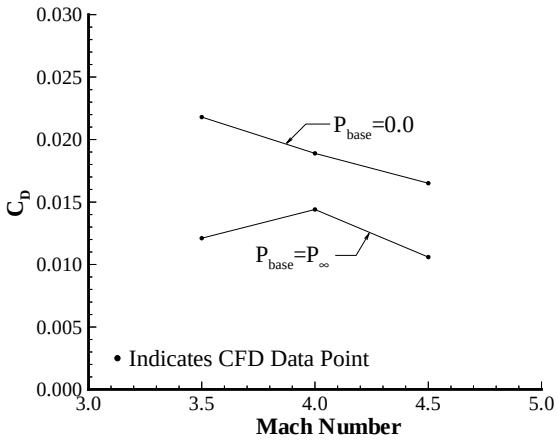

Figure 6. Mach number effect on C_D for waverider from CFD Predictions at α=0.0.

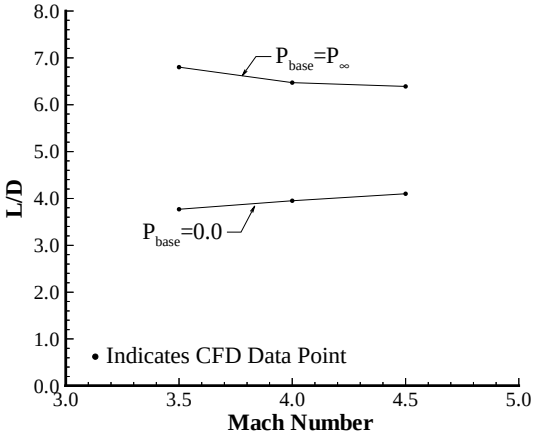

Figure 7. Mach number effect on L/D for waverider from CFD predictions at α=0.0.

	P_{base} = 0			P_{base} = P_∞		
M_∞	C_L	C_D	L/D	C_{L2}	C_{D2}	L/D
3.5	0.0823	0.0218	3.77	0.0823	0.0121	6.80
4.0	0.0747	0.0189	3.95	0.0747	0.0144	6.47
4.5	0.0677	0.0165	4.10	0.0677	0.0106	6.39

Table 1: Lift and drag coefficients from integrated surface pressure predictions for waverider model for Mach 4.0 and off-design Mach numbers at 0^o angle of attack.

A comparison of the waverider and reference configuration flow fields shows some of the differences between the two models. Figure 8 shows solutions of the waverider and flat-top configurations at Mach 4.0 and 0^o angle of attack. Static pressure contours are shown for the centerline and the base of each model. The most notable difference is that the bottom-surface pressure values are considerably lower for the flat-top configuration than for the waverider model. An examination of the geometry reveals that the bottom surface of the flat-top configuration has a slight expansion, due to the method which was used to design this configuration. In contrast, the bottom surface of the waverider model has a compression surface. The solutions at the base of each model show that the shock is slightly detached for each configuration. This detachment is due to boundary-layer displacement and blunt leading-edge effects. The bottom-surface flow field is more uniform for the waverider as compared to the reference model and thus more attractive for propulsion integration.

An examination of solutions at higher angles of attack at Mach 4.0 show the same type of behavior. For example, static pressure contours at the centerline and base of the reference and waverider models at Mach 4.0 and 4^o angle of attack are shown in figure 9. The solutions at 0^o and 4^o angle of attack are representative of all the angles of attack studied in that for each case the bottom-surface pressure values are lower for the flat-top model than for the waverider. The shock detachment distance at the leading edge also increases as angle of attack increases.

The lower pressure values on the bottom surface of the flat-top configuration result in lower lift and drag values. The lift and drag coefficients from integrated surface pressure predictions for the waverider and flat-top models at Mach 4.0 are shown in tables 2 and 3, respectively. The predicted values are again presented with two methods of base-pressure correction. At all angles of attack studied, the predicted values of both lift and drag coefficients are lower for the flat-top model than for the waverider. The performance characteristics of each configuration are examined by presenting the lift and drag predictions as a function of angle of attack and the lift-to-drag ratios as a function of lift coefficient.

The predicted and experimental lift and drag characteristics of each configuration at various angles of attack are shown in figures 10 through 14 for the design Mach number

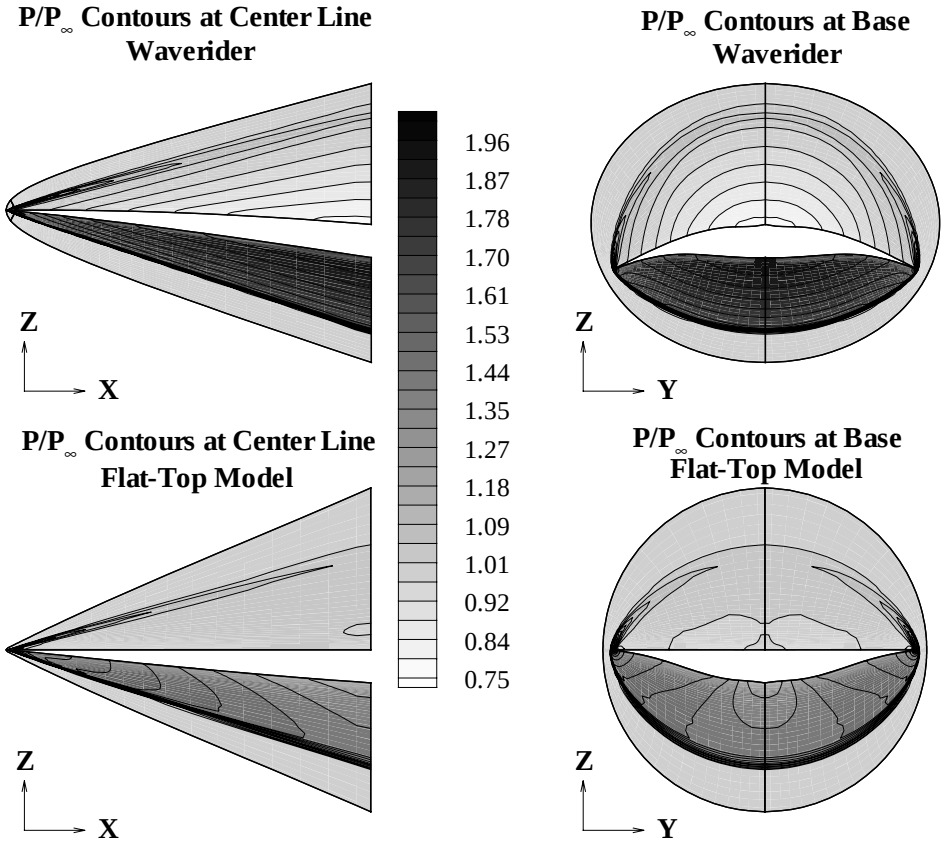

Figure 8. TLNS/PNS Solutions at M_∞=4.0, α=0.0^o

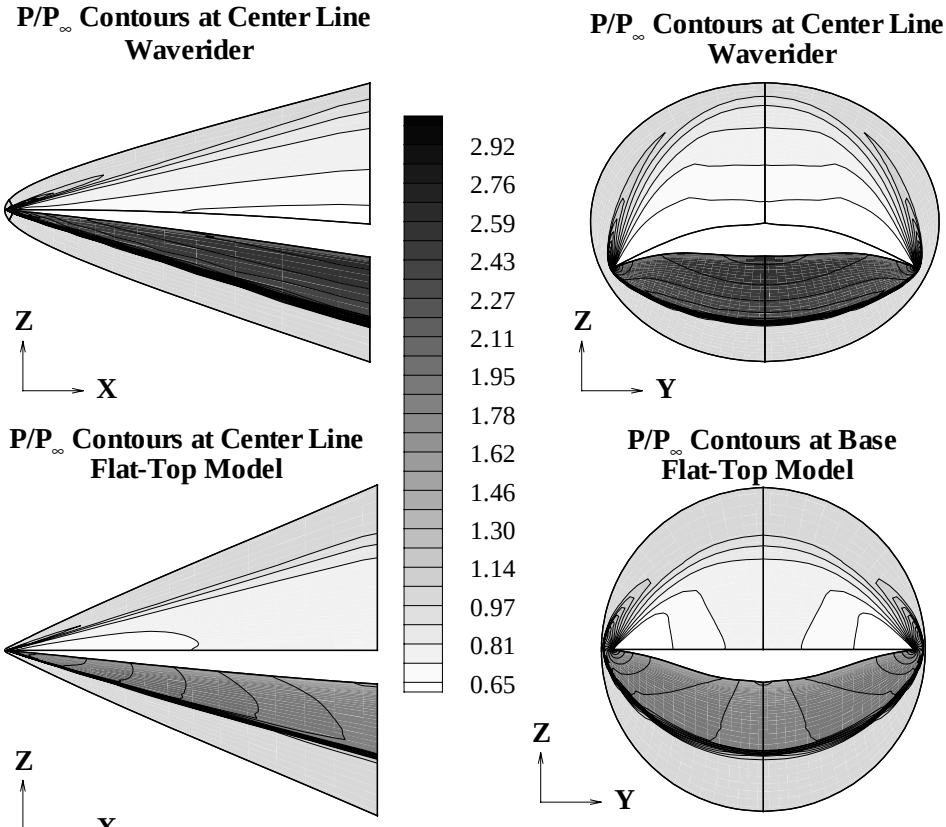

Figure 9. TLNS/PNS Solutions at M_∞=4.0, α=4.0

	$P_{base} = 0$			$P_{base} = P_\infty$		
α	C_L	C_D	L/D	C_{L2}	C_{D2}	L/D
0.0	0.0747	0.0189	3.95	0.0747	0.0115	6.45
1.0	0.0933	0.0218	4.28	0.0934	0.0144	6.47
2.0	0.1136	0.0264	4.30	0.1139	0.0190	5.99
3.0	0.1344	0.0307	4.38	0.1283	0.0233	5.56
4.0	0.1553	0.0364	4.27	0.1558	0.0290	5.37
6.0	0.2196	0.0554	3.96	0.2204	0.0480	4.59
10.0	0.3155	0.0982	3.21	0.3168	0.0909	3.39

Table 2: Lift and drag coefficients from integrated surface pressure predictions for waverider model at Mach 4.0 and selected angles of attack.

of 4.0. The variation of lift coefficient with angle of attack is presented in figure 10. This figure shows that the lift coefficient values for the waverider model are higher than those for the flat-top model at each angle of attack. These results are expected based on the predicted pressure values in the computational solutions. Good agreement is generally obtained between the CFD solutions and the experimental values. The drag coefficient data are presented in figure 11 assuming both zero base pressure and freestream base pressure. In both cases, higher drag values are shown for the waverider model

	$P_{base} = 0$			$P_{base} = P_\infty$		
α	C_L	C_D	L/D	C_{L2}	C_{D2}	L/D
0.0	0.0476	0.0155	3.07	0.0476	0.0081	5.87
1.0	0.0616	0.0165	3.73	0.0617	0.0092	6.74
2.0	0.0804	0.0192	4.19	0.0807	0.0118	6.82
3.0	0.0992	0.0226	4.39	0.0996	0.0152	6.53
4.0	0.1178	0.0268	4.40	0.1183	0.0194	6.11
6.0	0.1684	0.0399	4.22	0.1692	0.0325	5.20
10.0	0.2473	0.0716	3.45	0.2487	0.0644	3.86

Table 3: Lift and drag coefficients from integrated surface pressure predictions for Flat-Top Reference model at Mach 4.0 and selected angles of attack.

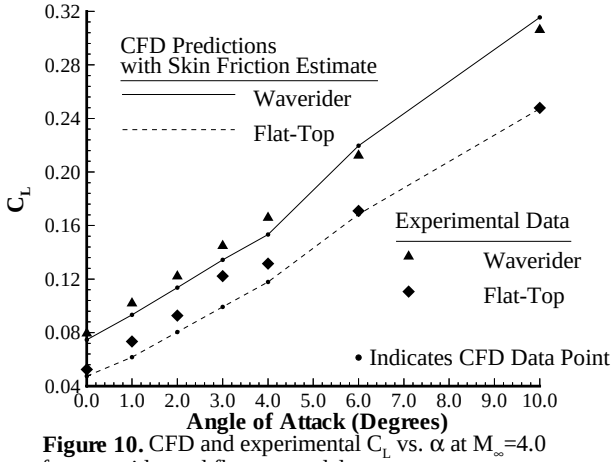

Figure 10. CFD and experimental C_L vs. α at M_∞=4.0 for waverider and flat-top model.

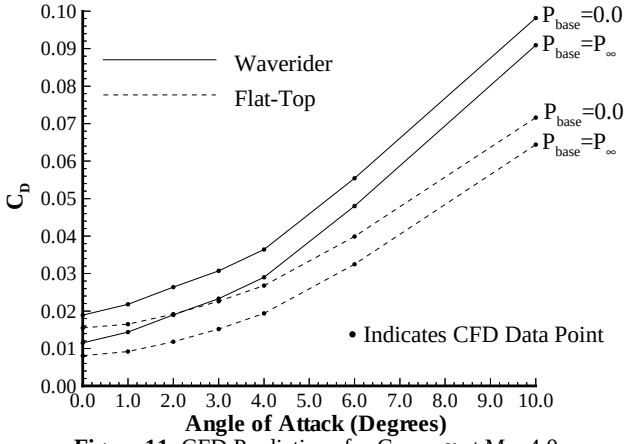

Figure 11. CFD Predictions for C_D vs. α at M_∞=4.0

at each angle of attack. The drag values for the waverider also increase more rapidly as the angle of attack increases. A comparison of drag coefficient values between CFD and experimental data for the case of base pressure equal to freestream pressure is shown in figure 12. Again, good agreement is generally obtained between CFD results and experimental data.

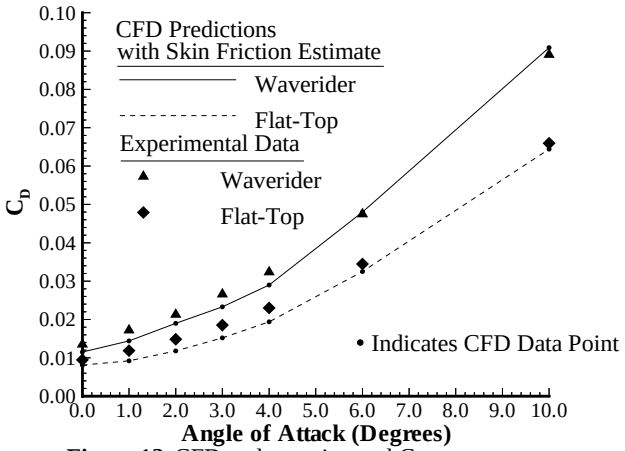

Figure 12. CFD and experimental C_D vs. α at M_∞=4.0 with P_{base}=P_∞.

The lift-to-drag ratio as a function of angle of attack at Mach 4.0 assuming zero base pressure is presented in figure 13. For this case, the maximum lift-to-drag ratio for the waverider occurs at an angle of attack of 3^o and for the flat-top configuration, at 4.0 degrees. The maximum lift-to-drag ratio of the flat-top model is less than 1 percent higher than that for the waverider model. The lift-to-drag ratio for both configurations are presented in figure 14 assuming a base

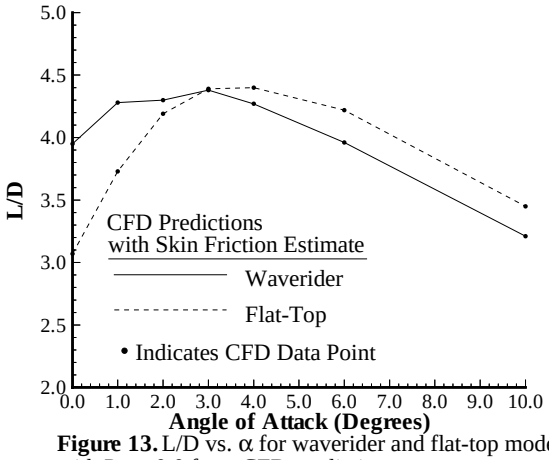

Figure 13. L/D vs. α for waverider and flat-top model with P_{base}=0.0 from CFD predictions.

pressure equal to freestream pressure. Using this method, the predicted maximum lift-to-drag ratio occurs at 1^o angle of attack for the waverider and at 2^o angle of attack for the flat-top model. The predicted maximum lift-to-drag ratio for the flat-top model is approximately 5.4 percent higher than that of the waverider model. The experimental values for lift-to-drag ratio are also shown in figure 14. In general, the lift-to-drag values from CFD solutions are higher than the experiment, especially for the flat-top model and the same trends are observed in the experiment and CFD results.

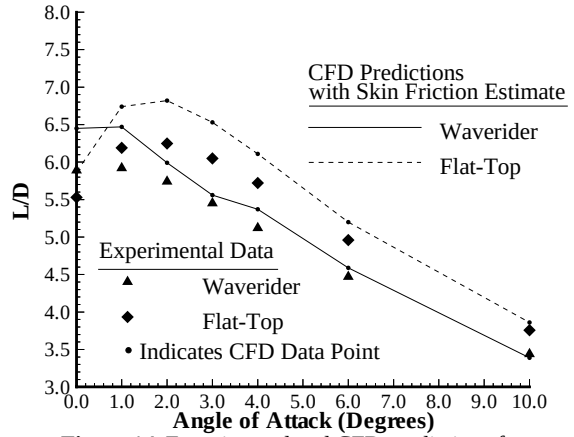

Figure 14. Experimental and CFD predictions for L/D vs. α at M_∞=4.0 with $P_{base}=P_\infty$.

The lift-to-drag ratio as a function of lift coefficient is presented in figure 15 assuming a base pressure equal to zero and in figure 16 assuming a base pressure equal to freestream pressure. The experimental data are included in figure 16 for comparison purposes. For small values of lift, the flat-top model has a higher lift-to-drag ratio than the waverider. For lift coefficient above 0.17, the waverider shows better performance. These results also show that the flat-top model has a higher maximum lift-to-drag ratio, but it occurs at a lower lift coefficient.

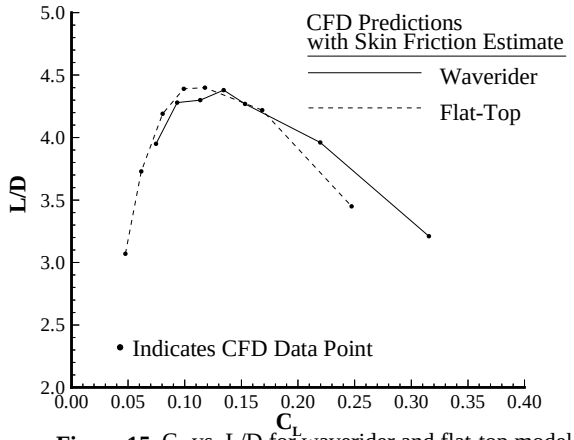

Figure 15. C_L vs. L/D for waverider and flat-top model with P_{base}=0.0 from CFD predictions.

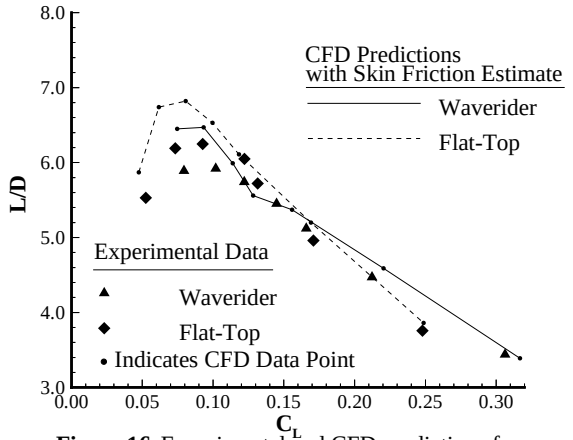

Figure 16. Experimental and CFD predictions for C_L vs. L/D with $P_{base}=P_\infty$.

Interpretations

Several conclusions can be made by the comparison between computational solutions of both configurations and between computational solutions and experimental data. The waverider configuration has higher lift than the reference flat-top configuration for all conditions investigated. However, the flat-top model has a higher lift-to-drag ratio at some points and a higher maximum lift-to-drag ratio than the waverider model due to relatively lower drag. In other words, at most values of lift coefficient, the drag coefficient is lower for the flat-top model than for the waverider, due to the lower bottom-surface pressures. This results in a higher lift-to-drag ratio for the flat-top model at most conditions. The improved performance of the flat-top model over that of the waverider is not due to the flat top surface, but rather to the shape of the bottom surface. For the configurations investigated herein, the bottom surface of the flat-top model has a slight expansion and therefore, lower surface pressure.

The results also illustrate that the type of base pressure assumed has a significant effect on the relative performance of the two configurations. The differences in lift-to-drag ratio are much greater when freestream pressure is assumed at the base than when zero base pressure is assumed. In comparing two configurations to assess their suitability for integration into a practical hypersonic vehicle, the assumption of zero base pressure may be more appropriate since the blunt base will most likely be eliminated in any representative vehicle design by the addition of control surfaces. However, it would be appropriate to use the assumption of freestream pressure acting at the base in the design process in order to avoid widely varying solutions due to changing base areas.

The flat-top model exhibits the same shock attachment properties as the waverider model because the planform shapes of the two configurations are identical. Based on the improved performance of the flat-top model, it can be concluded that the basic physical effect that gives the waverider its advantage in aerodynamic performance over conventional hypersonic vehicles is the shock attachment caused by the shape of the leading edge. Designing the bottom surface as a streamsurface improves flow-field uniformity and makes the waverider a more attractive candidate for scramjet integration, but does not enhance the aerodynamic performance. The bottom surface of a waverider can be altered somewhat without a large decrease in lift-to-drag ratio. This suggests that altering the lower surface of a waverider configuration to integrate engine components should not degrade the performance of the vehicle significantly as long as the planform shape is maintained.

Conclusions

A computational study was conducted to better understand the results obtained from an experimental investigation of a Mach 4 waverider and a reference flat-top configuration. The results from this experiment contradicted waverider design theory by showing that the flat-top configuration had a higher maximum lift-to-drag ratio than the waverider. The waverider model was designed using an optimization routine which includes an estimate for skin friction in the optimization process. The reference model was designed by adjusting the top surface of the waverider to obtain a flat surface, while maintaining the same planform shape and cross-sectional area distribution.

Viscous solutions were obtained for both configurations and lift and drag predictions were obtained from these solutions by integrating surface pressure values and including an estimate for skin friction. Solutions of the waverider at the design Mach number and selected off-design Mach numbers showed that the off-design performance of the waverider does not degrade significantly at off-design conditions. The bottom-surface pressures of both the waverider and flat-top model at Mach 4.0 and selected angles of attack showed that the bottom surface of the flat-top model provides a slight expansion, in contrast to the waverider bottom surface, which acts as a compression surface. The result is that the lift and drag predictions for the flat-top model are much lower than those for the waverider model. These characteristics result in higher lift-to-drag ratios for the flat-top model for lift coefficients lower than 0.17 and a higher maximum lift-to-drag ratio. However, the differences in performance between the two configurations are primarily due to the shape of the bottom surface independent of the top surface. The results also indicate that the performance of each configuration is significantly affected by the type of base pressure correction used.

The CFD results also show that the reference configuration exhibits the same shock attachment properties as the waverider, due to the planform shapes being identical. The results from this study suggest that the leading-edge shock attachment, which is a result of the planform shape, is the main effect that gives waveriders their high lift-to-drag ratios. The performance of the configuration should not degrade significantly if the bottom surface is altered from the optimized waverider design, as long as the planform shape is maintained.

References

1. Bowcutt, Kevin G. and Anderson, John D. “Viscous Optimized Hypersonic Waveriders,” AIAA Paper 87-0272, AIAA 24th Aerospace Sciences Meeting, Reno, NV, January 12-15, 1987.

2. O’Neill, Mary Kae and Lewis, Mark J. “Optimized Scramjet Integration on a Waverider,” *Journal of Aircraft*, vol. 29, no. 6, November-December 1992, pp. 1114-1121.

3. Bauer, Steven X.S. “Analysis of Two Viscous Optimized Waveriders,” First International Hypersonic Waverider Symposium, University of Maryland, College Park, MD, October 1990.

4. Takashima, Naru and Lewis, Mark J. “Navier-Stokes Computation of a Viscous-Optimized Waverider,” AIAA Paper 92-0305, AIAA 30th Aerospace Sciences Meeting, Reno, NV, January 6-9, 1992.

5. Corda, Stephen and Anderson, John D. “Viscous Optimized Hypersonic Waveriders Designed from Axisymmetric Flow Fields,” AIAA Paper 88-0369, AIAA 26th Aerospace Sciences Meeting, Reno, NV, January 11-14, 1988.

6. McGrory, William D., Huebner, Lawrence D., Slack, David C. and Walters, Robert W. “Development and Application of GASP 2.0,” AIAA Paper 92-5067, AIAA 4th International Aerospace Planes Conference, Orlando, FL, December 1-4, 1992.

7. Jones, Kevin D. “Numerical Simulation of High-Speed Flows About Waveriders with Sharp Leading Edges,” *Journal of Spacecraft and Rockets*, vol. 29, no. 5, September-October 1992, pp. 661-667.

8. Steinbrenner, John P., Chawner, John R. and Fouts, Chris L. *The GRIDGEN 3D Multiple Block Grid Generation System*, Report number WRDC-TR-90-3022, Flight Dynamics Laboratory, Wright Research and Development Center, Wright-Patterson Air Force Base, OH, July 1990.

9. Richardson, Pamela F. and Parlette, Edward B. “Comparison Between Experimental and Numerical Results for a Research Hypersonic Aircraft”, *Journal Of Aircraft*, vol. 27, no. 4, April 1990, pp. 300-305.

10. Sommer, Simon C. and Short, Barbara J. *Free-Flight Measurements of Turbulent-Boundary-Layer Skin Friction in the Presence of Severe Aerodynamic Heating at Mach Numbers From 2.8 to 7.0*. NACA TN-3391, March 1955.